**Showcasing research from the TIFR-Centre for Interdisciplinary Sciences (TCIS), Hyderabad, India and the CSIR-Central Electrochemical Research Institute (CSIR-CECRI), Karaikudi, India.**

The improved electrochemical performance of cross-linked 3D graphene nanoribbon monolith electrodes

This work demonstrates the augmented electrochemical performance of 3-dimensional (3D) monolith electrode made of 2-dimensional (2D) graphene nanoribbons (GNRs). GNRs are benchmarked materials for electrochemical applications while here the authors demonstrate the efficacy of 3D electrodes over 2D electrodes, enlightening the importance of electrode engineering. One of the authors T. N. Narayanan is a faculty member at TIFR-Centre for Interdisciplinary Sciences and Vineesh is a Ph.D. student at CSIR-CECRI. S. Alwarappan is a Senior Scientist at CSIR-CECRI.

ROYAL SOCIETY OF **CHEMISTRY**

www.rsc.org/nanoscale

The improved electrochemical performance of cross-linked 3D graphene nanoribbon monolith electrodes†
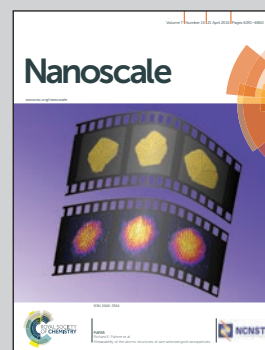
Thazhe Veettil Vineesh,[a] Subbiah Alwarappan*[a] and Tharangattu N. Narayanan*[b]

Technical advancement in the field of ultra-small sensors and devices demands the development of novel micro- or nano-based architectures. Here we report the design and assembly of cross-linked three dimensional graphene nanoribbons (3D GNRs) using solution based covalent binding of individual 2D GNRs and demonstrate its electrochemical application as a 3D electrode. The enhanced performance of 3D GNRs over individual 2D GNRs is established using standard redox probes – $[Ru(NH_3)_6]^{3+/2+}$, $[Fe(CN)_6]^{3-/4-}$ and important bio-analytes – dopamine and ascorbic acid. 3D GNRs are found to have high double layer capacitance (2482 $\mu F\ cm^{-2}$) and faster electron transfer kinetics; their exceptional electrocatalytic activity towards the oxygen reduction reaction is indicative of their potential over a wide range of electrochemical applications. Moreover, this study opens a new platform for the design of novel point-of-care devices and electrodes for energy devices.

1. Introduction

Development of three dimensional (3D) hierarchical structures from nano-building blocks has shown a tremendous impact on recent research due to their practical applications in the fields of environmental protection, gas storage and energy.[1–3] However, covalent linkage between individual nano-blocks, without losing their distinctive properties like high surface area, electronic or electrochemical properties while constructing bulk macroscopic structures, has been identified as challenging.[4] Ultra-low density graphene and graphene oxide (GO) sponges,[5,6] graphene and graphene oxide hydrogels,[7] carbon nanotube sponges,[8] and other 2D material-based sponges[9] are some of the recently developed macroscopic 3D structures showing promising applications.

Recently, as initiated by some of the authors, the covalent linkages between individual GO sheets were achieved by using simple chemistry, leading to the synthesis of highly stable interconnected bulk 3D structures.[10] Graphene nanoribbons (GNRs), a new carbonaceous material with a high length-to-breadth ratio, also received tremendous scientific attention, mainly due to their tunable electronic properties with high aspect ratio control,[11] as well as their unique electrochemical

properties with immense benefits in various electrochemical applications.[14] Zhang *et al.*[12] have developed GNR-based electrochemical systems like batteries and supercapacitors which show better performance than other carbon counterparts. GNRs are advantageous compared to GO mainly in three aspects: (a) they are relatively more active than GO in the electrochemical response owing to their highly active edge planes;[13] (b) due to the presence of large area active edge planes, inter-GNR covalent linkage is easier than in GO and this in turn can give ultra-low bulk density GNR sponges with a minimum amount of GNRs; and (c) structurally more uniform GNRs with identical dimensions are easily achievable, whereas chemically derived GO sheets show a huge variation in their size distribution. In short, GNR-based 3D structures are expected to have higher hierarchical ordered morphology with more uniform porosity, hence they are interesting candidates for their potential in constructing electrochemical electrodes.

The planarity of conventional electrochemical electrodes limits the active surface area for electrochemical reactions. The use of nanomaterials with high surface area has been attempted to address this shortcoming of planar electrodes.[15] However, modifications of electrodes with these nanomaterials have provided barely nominal changes in their electrochemical response due to the limitations of supporting planar electrodes. This study introduces a 3D electrode for electrochemical reactions, whose morphology is developed from 2D GNRs by chemical cross-linking, hereafter called 3D GNRs. In addition, this study probes the electron transfer kinetics of these new electrodes. The performance of 3D GNRs in comparison with

[a]CSIR-Central Electrochemical Research Institute (CSIR-CECRI), Karaikudi-630006, India. E-mail: salwarap@gmail.com
[b]TIFR-Centre for Interdisciplinary Sciences, Tata Institute of Fundamental Sciences, Hyderabad - 500 075, India. E-mail: tn_narayanan@yahoo.com, tnn@tifrh.res.in
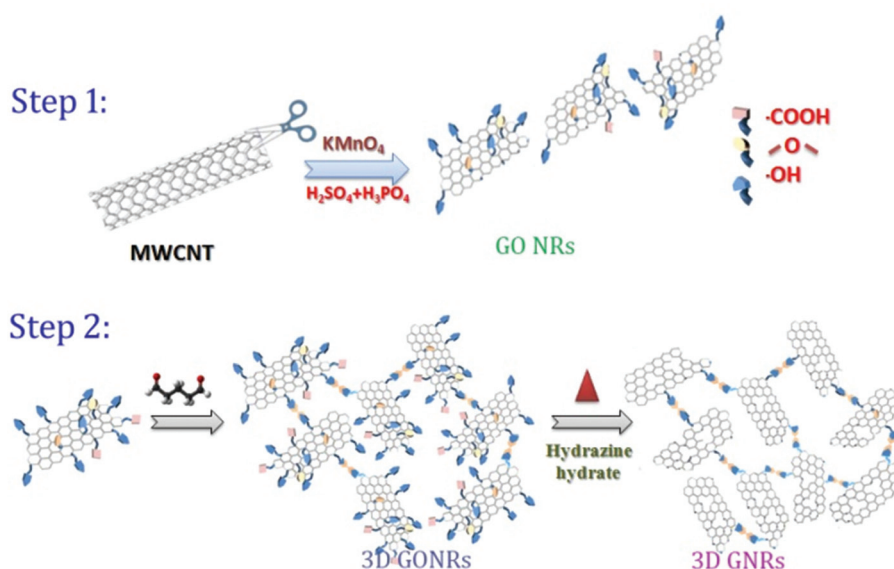†Electronic supplementary information (ESI) available. See DOI: 10.1039/c4nr07315k

Fig. 1 Schematic of the synthesis of 3D GNRs: step 1: synthesis of GO nanoribbons (GONRs) from MWCNTs; step 2: synthesis of 3D GONRs using GONRs with a GAD cross-linking agent (the chemical structure of GAD shown above the arrow) and subsequent thermal reduction at 50 °C under a hydrazine hydrate atmosphere leading to the formation of 3D GNRs. The −OH groups in the GONR sheets will bind with GAD *via* hemiacetal linkage to contribute large scale cross-linking between individual GONRs as shown in step 2. The lyophilisation of the resulting solution leads to the formation of porous solids as shown in Fig. 2A and C.

2D GNRs is investigated using standard redox probes such as inner- and outer-sphere redox mediators – $[Ru(NH_3)_6]^{3+/2+}$, $[Fe(CN)_6]^{3-/4-}$ and bio-analytes – dopamine and ascorbic acid. Furthermore, electrocatalytic and supercapacitance applications of these 3D electrodes are studied.

2.   Synthesis of GNRs and 3D GNRs

2.1   GONR synthesis

GONR was synthesized using a well-established technique of oxidative unzipping of MWCNTs employing $KMnO_4$ under acidic conditions.[16] 100 mg of MWCNTs (purchased from http://www.cheaptubes.com) was dispersed in 36 mL of H_2SO_4. This mixture was stirred for 1 hour (this will help in removing the metallic catalyst present in MWCNTs and stirring will result in uniform suspensions). 4 mL of H_3PO_4 (so that the volume ratio of H_2SO_4/H_3PO_4 is 9 : 1) was added to this mixture and stirring was continued for next 15 minutes. 800 mg $KMnO_4$ was then added to the mixture (8 weight equivalent of MWCNTs). The temperature was raised to 65 °C and stirring was continued for 2 hours. It was noticed that prolonged and vigorous sonication/stirring of this mixture at elevated temperatures leads to the formation of completely broken tubes (flake size of 10–15 nm with irregular shape). The mixture was cooled down to room temperature and the reaction mixture was poured into an ice bath containing hydrogen peroxide (∼5 mL). The resulting precipitate was filtered and washed several times using water and HCl in a consecutive and cyclic manner. The material is dispersed and coagulated using ethanol and ether (similar to GO synthesis) and the powder is filtered and dried using a vacuum oven.

2.2   3D GONR synthesis

Dried GONR powder is dispersed in water and a 22 mM glutaraldehyde (GAD) solution is added into this dispersion and the resulting solution was stirred for 3 hours. The solution was poured into some regular shaped dies and is freeze dried using a lyophilizer. The resulting material is a highly porous solid with a macroscopic shape of the die used for casting.

2.3   3D GNR synthesis

The 3D GONR solid is reduced using hydrazine hydrate at a temperature of 50 °C, keeping the sample in a vacuum oven for 12 hours. The schematic of the whole procedure is shown in Fig. 1.

3.   Development of GNR and 3D GNR electrodes

The working electrodes, GNR and 3D GNR, were developed in the following manner: a glassy carbon electrode (GCE, 3 mm diameter) was polished using 0.3 μm and 0.05 μm alumina slurries, and then cleaned under sonication for 5 minutes in acetone and doubly distilled water successively. GNRs (2 mg) were dispersed in a DMF (1 mL) solution after sonication to obtain a homogenous solution. The GNR based electrodes were prepared by drop casting the GNR solution (5 μL) on the GC substrate and the electrodes were then dried at ambient temperature. 3D GNR based electrodes were also prepared in a

similar manner. The morphology of the coated electrodes was studied using a scanning electron microscope, where the GNR modified electrode showed a planar structure while the 3D GNR modified electrode exhibited a porous interconnected structure with full coverage of GCE.

4. Analytical instruments

Cyclic voltammograms (CVs) were measured in a three electrode configuration using the CH Instrument model 1000A potentiostat. Ag/AgCl and platinum foil were used as the reference and counter electrodes, respectively. All experiments were carried out at room temperature. Raman spectra were obtained using a confocal microprobe Raman system (Renishaw, RM2000). From the XRD pattern of 3D GONRs, the prominent (002) peak at 10 indicates that the interplanar distance is still more than 6 Å (Fig. S1†), like GNR powders, even after the chemical treatment. Transmission electron microscopy (TEM) images were obtained with a Philips CM 200 transmission electron microscope operating at an accelerating voltage of 200 kV. Field emission scanning electron microscopy (FESEM) images of GNRs and 3D GNRs were obtained from a field emission SEM system (FEI Quanta 400 ESEM FEG). XPS analysis was done using a PHI 5000 Versa Probe ULVAC instrument.

5. Results and discussion

The morphology of GNRs is shown in Fig. 2A (FESEM) and 2C (TEM). The width of the nanoribbons is approximately 150 nm and the length is of several micrometres. As is reported,[16] GONRs contain various oxygen bearing functional groups (mostly carboxyl, hydroxyl and epoxy groups) similar to GO. A similar mechanism as we reported for GO[10] has been attempted to connect individual GONRs. The FESEM and TEM images of the resulting interconnected and porous 3D GONRs are shown in Fig. 2C and 2D, respectively. The XRD spectrum (Fig. S1†) indicates that the 3D GONRs also show the interplanar (002) distance of ~6 Å without the restacking of layers even after chemical treatment. These 3D GONRs are reduced using hydrazine hydrate vapour at 50 °C. The resulting 3D GONRs and GONRs were compared for their chemical structure using infrared spectroscopy (FT-IR) (Fig. 2F). The additional –CH stretching at 2900 cm^{-1} is observed in the FT-IR spectrum of 3D GONRs, corresponding to the formation of hemiacetal linkages between individual GONRs.[16] The intensities of the Raman spectra of 3D GONRs and 3D GNRs are compared (Fig. 2E) and an increase in the ratio of D and G for 3D GNRs (I_D/I_G = 1.06) is an indication of the reduction of 3D GONRs (I_D/I_G = 0.87). Moreover 3D GNRs have an enhanced surface area (~500 m^2 g^{-1}) with a macro- and mesoporous structure compared to the parent GNRs (~140 m^2 g^{-1}, Fig. S3 and S4†). In order to identify the oxygen functionalities of 3DGONR and 3D GNR, we performed X-ray photoelectron spectroscopy (XPS) analysis on both the samples. The high resolution C1s spec-
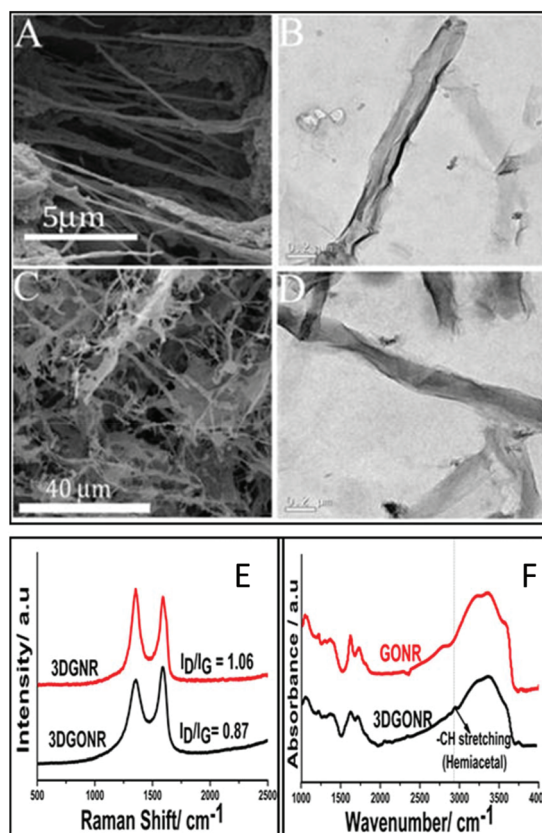

Fig. 2 (A & C) FESEM images of GONRs (GONR) and 3D GONRs (3DGONR), (B & D) TEM images of GONRs and 3D GONRs, (E) Raman spectra of 3D GONRs and 3D GNRs, (F) FT-IR spectra of GONRs and 3DGONRs.

trum exhibited well defined double peak formation which indicates the extreme oxidation of the 3DGONRs (Fig. S2†). After deconvolution the sp^2 peak of the C1s spectrum centred at 284.5 eV. In addition to the sp^2 graphite component, we found three broad components to account for the overlapping C1s features. The component at 285.3 eV is assigned to C atoms directly bonded to oxygen in hydroxyl (–OH) configurations. The component at 286.9 eV is attributed to the epoxide group (C–O–C), and the component at 288.5 eV is related to carbonyl (>C=O) or carboxyl groups (HO–C=O). After the reduction with hydrazine vapour, the C1s spectrum of 3D GNR shows three peaks which correspond to C=C, C–OH or C–O–C and C=O (carbonyl or carboxylic). The low intensity of C–OH or C–O–C and C=O indicates the reduction of 3D GONR to 3D GNR.[17–22]

5.1. Electrochemical behaviour of GNRs and 3D GNRs towards different redox probes

The electrochemical response being highly sensitive to the physical properties of the surface, background cyclic voltammograms are measured using GNR and 3D GNR electrodes (Fig. 3A). Detailed electron transfer kinetics of these electrodes are studied using "inner sphere" and "outer sphere" redox probes (mediators). These probes will distinguish between
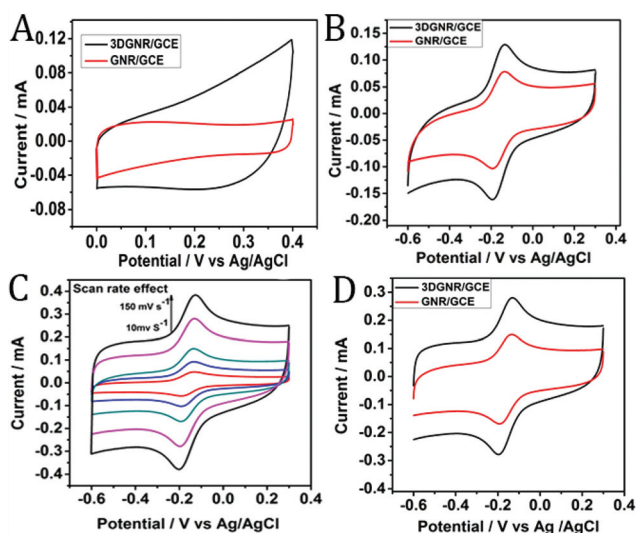
Fig. 3 CVs of GNR and 3D GNR modified GC electrodes: (A) in 1.0 M KCl, (B) 5.0 mM $[Ru(NH_3)_6]^{3+/2+}$ in 1.0 M KCl, (C) the effect of scan rate on the 3D GNR modified electrode in 5.0 mM $[Ru(NH_3)_6]^{3+/2+}$ in 1.0 M KCl, (D) 5.0 mM $[Fe(CN)_6]^{3-/4-}$ in 1.0 M KCl, at a scan rate of 50 mV s^{-1}.

outer sphere and inner sphere electron transfer processes, which in turn will unravel the roles of the density of states (DOS) and surface functionalities of the electrode materials in deciding the net electron transfer rates between electrodes and molecules. Fast electron transfer rates (rate constants, as inferred from the peak potential difference, ΔE_p) rely on the efficiency of electrodes in developing highly sensitive devices from them. In the case of outer sphere redox mediators such as $[Ru(NH_3)_6]Cl_3$ and $K_2[(IrCl_6)]$, the rate constant is not affected by their surface microstructures, oxygen functionalities, and adsorbed species on the electrode surfaces.[23] In other words, no chemical interactions or adsorption with the electrode surface or with a functional group in the surface are involved in the case of the outer sphere redox mechanism. In this case, the electrode merely serves as a source or a sink of electrons and is affected only by the electronic structure (DOS) of the electrode.

The ruthenium redox couple $[Ru(NH_3)_6]^{3+/2+}$ is an outer-sphere redox couple and the cyclic voltammograms measured for this redox couple gives ΔE_p values of (60 ± 1.3 mV, N = 5) and (61 ± 1.5 mV, N = 5) respectively for 3D GNRs and GNRs, as shown in Fig. 3B. Though the difference in (ΔE_p) is nominal the current increases from 72 µA (for GNRs) to 102 µA (for 3D GNRs) (in all the experiments, the loading amounts of both the materials are kept constant, 142.8 µg cm^{-2}). This increase in peak current is due to the increase in surface area and augmented charge transfer kinetics through the 3D GNR network. This redox system is also selected for investigating the effect of scan rate on peak current values to understand the diffusion mechanism (Fig. 3C). The oxidation and reduction peak currents increase linearly with the square root of the scan rate in the cases of both GNRs and 3D GNRs (Fig. S3†), indicating that the reactions are controlled by semi-infinite linear diffusion.[24]

Conversely, inner sphere redox mediators are termed as surface sensitive probes, and here the rate constant is strongly influenced by surface chemistry and surface microstructures. Another redox probe, $[Fe(CN)_6]^{3-/4-}$, is an ideal quasi reversible mediator for carbon electrodes.[25] Fig. 3D shows the cyclic voltammograms for $[Fe(CN)_6]^{3-/4-}$ using GNR and 3D GNR electrodes. The (ΔE_p) values are calculated as (61 ± 1.5 mV, N = 5) and (63 ± 1.7 mV, N = 5) respectively for 3D GNRs and GNRs. A lower ΔE_p value of 61 mV for 3D GNRs indicates that the fast electron transfer kinetics of parent GNRs is not adversely affected by the interconnecting network.

5.2. Electrochemical sensing of ascorbic acid and dopamine

The fast electron transfer process occurring in these electrodes along with an enhanced peak current (surface area) motivated for the development of biosensors with these electrodes. An important neurotransmitter like dopamine (DA) and its coexistent ascorbic acid (AA) are vital bioanalytes that need to be monitored.[26,27] Cyclic voltammograms are measured with both AA and DA using 3D GNRs and GNRs (details are given in Fig. 4A and B) and in both the cases, 3D GNRs showed negative shifts in potential with a large increase in peak currents. Unique electronic properties, high surface area and fast electron transfer through the 3D network are responsible for these augmented performances of 3D GNRs in comparison with their parent GNRs or the benchmarked GCE.

5.3. Capacitance and electrocatalytic oxygen reduction

3D GNRs and 2D GNRs are studied for their capacitance measurements, and the cyclic voltammograms in alkaline medium are shown in Fig. 4C. The capacitance values are calculated as 2482 µF cm^{-2} and 1942 µF cm^{-2} for 3D GNRs and GNRs respectively. This study also indicates the enormous surface area enhancement of 3D GNRs and identifies them as a potential candidate for the supercapacitor applications. The oxygen reduction reaction (ORR) is important in various
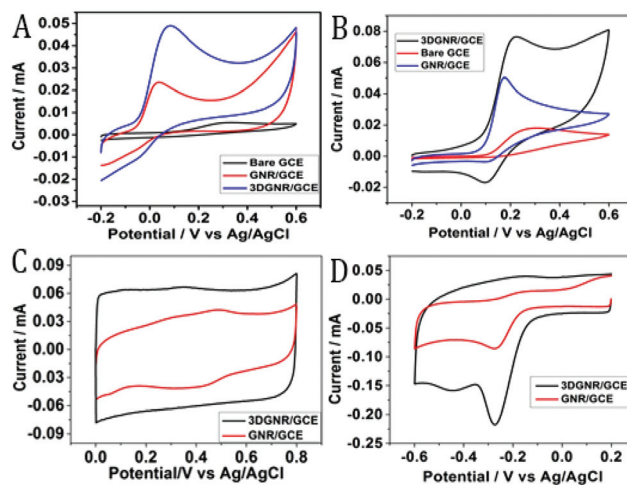

Fig. 4 CVs recorded with GNRs and 3D GNRs in (A) 1 mM AA and (B) 1 mM DA in 0.1 M pH 7 phosphate buffer, (C) in 0.1 M NaOH, (D) ORR in 0.1 M NaOH solution saturated with oxygen, scan rate 50 mV s^{-1}.
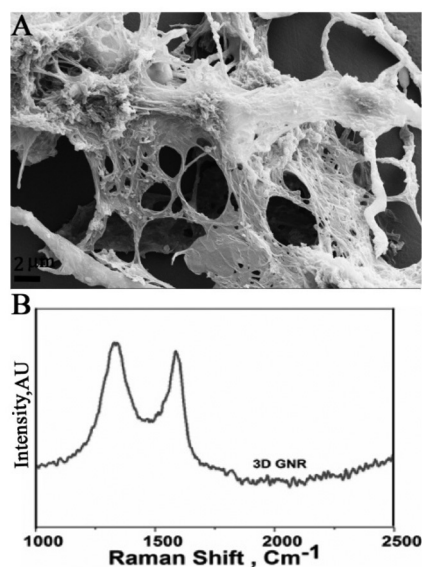
Fig. 5 (A) FESEM image and (B) Raman spectrum of 3D GNRs, after the electrochemical performances (after the 10th cycle).

supercapacitors and their performance towards different redox probes respectively indicate enhanced surface area and faster electron transfer for GNR based 3D electrodes compared to bare 2D GNRs. The high surface area and fast electron transfer have proven advantageous for ORR and sensing (AA and DA). Hence this study puts forward a new class of 3D engineered electrodes with immense benefits in many electrochemical processes, and opens new avenues for the design of novel sensors and devices from existing materials by engineering their morphologies.

Acknowledgements

electrochemical energy conversion processes such as fuel cells, metal air batteries and corrosion processes.[28,29] Fig. 4D shows the cyclic voltammograms for ORR at GNR and 3D GNR electrodes. Two reduction peaks are observed in both the electrodes, which indicate that the electrochemical reduction of oxygen occurs in two processes – first in the production of HO_2^- and later in its reduction to H_2O. In the case of 3D GNR electrodes, there is an increase in the peak current compared with the GNR modified electrodes with a slight change in the onset potential, which suggests the faster electron transfer kinetics for ORR on 3D GNRs in comparison with bare GNRs.[30]

In order to check the structural integrity/stability of 3D GNR based electrodes after electrochemical performances, FESEM and Raman studies are performed on 3D GNRs after the 10th cycle (after scratching the 3D GNRs from the GCE). The FESEM image (Fig. 5A) indicates that the 3D cross-linkage is intact even after a number of electrochemical cycles (after 10 cycles) showing the stability of the electrodes. Furthermore, the Raman spectrum of the 3D GNRs (Fig. 5B) proves the presence of graphitic D and G bands, and their intensities/peak positions are not affected by the electrochemical performances in comparison with the parent 3D GNRs (Fig. 2E). Hence these studies prove the stability of 3D GNR based electrodes towards various electrochemical reactions.

6. Conclusions

GNR-based 3D electrodes have been developed and studied for their performance in various electrochemical reactions. 3D GNR-based electrodes are found to be well interconnected and porous, and they show structural stability (even after extensive sonication and electrochemical performances). Studies on

Notes and references

1 D. P. Hashim, N. T. Narayanan, J. M. Romo-Herrera, D. a. Cullen, M. G. Hahm, P. Lezzi, J. R. Suttle, D. Kelkhoff, E. Muñoz-Sandoval, S. Ganguli, et al., Sci. Rep., 2012, 2, 363.

2 R. Kumar, V. M. Suresh, T. K. Maji and C. N. R. Rao, Chem. Commun., 2014, 50, 2015.

3 M. G. Hahm, A. Leela Mohana Reddy, D. P. Cole, M. Rivera, J. a. Vento, J. Nam, H. Y. Jung, Y. L. Kim, N. T. Narayanan, D. P. Hashim, et al., Nano Lett., 2012, 12, 5616.

4 X. Jiang, J. Zhao, Y.-L. Li and R. Ahuja, Adv. Funct. Mater., 2013, 23, 5846.

5 J. Biener, S. Dasgupta, L. Shao, D. Wang, M. a. Worsley, A. Wittstock, J. R. I. Lee, M. M. Biener, C. a. Orme, S. O. Kucheyev, et al., Adv. Mater., 2012, 24, 5083.

6 Z. Niu, J. Chen, H. H. Hng, J. Ma and X. Chen, Adv. Mater., 2012, 24, 4144.

7 H. P. Cong, X.-C. Ren, P. Wang and S. Yu, ACS Nano, 2012, 6, 2693.

8 X. Gui, J. Wei, K. Wang, A. Cao, H. Zhu, Y. Jia, Q. Shu and D. Wu, Adv. Mater., 2010, 22, 617.

9 W. Li, C. Tan, M. A. Lowe, H. D. Abruna and D. C. Ralph, ACS Nano, 2011, 5, 2264.

10 P. M. Sudeep, T. N. Narayanan, A. Ganesan, M. M. Shaijumon, H. Yang, S. Ozden, P. K. Patra, M. Pasquali, R. Vajtai, S. Ganguli, et al., ACS Nano, 2013, 7, 7034.

11 O. V. Yazyev, Acc. Chem. Res., 2013, 46, 2319.

12 L. L. Zhang, R. Zhou and X. S. Zhao, J. Mater. Chem., 2010, 20, 5983.

13 H. Kim, K. Lee, S. I. Woo and Y. Jung, Phys. Chem. Chem. Phys., 2011, 13, 17505.

14 D. A. C. Brownson, D. K. Kampouris and C. E. Banks, *Chem. Soc. Rev.*, 2012, **41**, 6944.

15 C. E. Banks and R. G. Compton, *Analyst*, 2006, **131**, 15.

16 D. K. James and J. M. Tour, *Macromol. Chem. Phys.*, 2012, **213**, 1033.

17 C. Mattevi, G. Eda, S. Agnoli, S. Miller, K. A. Mkhoyan, O. Celik, D. Mastrogiovanni, G. Granozzi, E. Garfunkel and M. Chhowalla, *Adv. Funct. Mater.*, 2009, **19**, 2577.

18 A. Bagri, C. Mattevi, M. Acik, Y. J. Chabal, M. Chhowalla and V. B. Shenoy, *Nat. Chem.*, 2010, **2**, 581.

19 D. Yang, A. Velamakanni, G. Bozoklu, S. Park, M. Stoller, R. D. Piner, S. Stankovich, I. Jung, D. A. Field and C. A. Ventrice, *Carbon*, 2009, **47**, 145.

20 C. Hontoria-Lucas, A. J. Lopez-Peinado, J. D. López-González, M. L. Rojas-Cervantes and R. M. Martin-Aranda, *Carbon*, 1995, **33**, 1585.

21 A. Barinov, L. Gregoratti, P. Dudin, S. L. Rosa and M. Kiskinova, *Adv. Mater.*, 2009, **21**, 1916.

22 Y. Q. Wang, F. Q. Zhang and P. M. A. Sherwood, *Chem. Mater.*, 1999, **11**, 2573.

23 P. Chen and R. L. McCreery, *Anal. Chem.*, 1996, **68**, 3958.

24 I. Streeter, G. G. Wildgoose, L. Shao and R. G. Compton, *Sens. Actuators, B*, 2008, **133**, 462.

25 L. Tang, Y. Wang, Y. Li, H. Feng, J. Lu and J. Li, *Adv. Funct. Mater.*, 2009, **19**, 2782.

26 G. U. Hoglinger, P. Rizk, M. P. Muriel, C. Duyckaerts, W. H. Oertel, I. Caile and E. C. Hirsch, *Nat. Neurosci.*, 2004, **7**, 726.

27 K. L. Davis, R. S. Kahn, G. Kao and M. Davison, *Am. J. Psychiatry*, 1991, **148**, 1474.

28 Z. L. Wang, D. Xu, J. J. Xu and X. B. Zhang, *Chem. Soc. Rev.*, 2014, **43**, 7746.

29 C. He, J. J. Zhang and P. K. Shen, *J. Mater. Chem. A*, 2014, **2**, 3231.

30 Z.-H. Sheng, H.-L. Gao, W.-J. Bao, F.-B. Wang and X.-H. Xia, *J. Mater. Chem.*, 2012, **22**, 390.